

# Core-shell *p-i-n* GaN nanowire LEDs by N-polar selective area growth\*

Matt D. Brubaker\*\*<sup>a</sup>, Kristen L. Genter<sup>a,b</sup>, Joel C. Weber,<sup>a</sup> Bryan T. Spann<sup>a</sup>, Alexana Roshko<sup>a</sup>, Paul T. Blanchard<sup>a</sup>, Todd E. Harvey<sup>a</sup>, Kris A. Bertness<sup>a</sup>

<sup>a</sup>Physical Measurement Laboratory, National Institute of Standards and Technology, 325 Broadway, Boulder, CO, USA 80305; <sup>b</sup>Department of Mechanical Engineering, University of Colorado, 1111 Engineering Drive, Boulder, CO USA 80309

## ABSTRACT

GaN nanowire LEDs with radial *p-i-n* junctions were grown by molecular beam epitaxy using N-polar selective area growth on Si(111) substrates. The N-polar selective area growth process facilitated the growth of isolated and high-aspect-ratio *n*-type NW cores that were not subject to self-shadowing effects during the subsequent growth of a conformal low-temperature Mg:GaN shell. LED devices were fabricated from single-NW and multiple-NW arrays in their as-grown configuration by contacting the *n*-type core through an underlying conductive GaN layer and the *p*-type NW shell via a metallization layer. The NW LEDs exhibited rectifying I-V characteristics with a sharp turn-on voltage near the GaN bandgap and low reverse bias leakage current. Under forward bias, the NW LEDs produced electroluminescence with a peak emission wavelength near 380 nm and exhibited a small spectral blueshift with increasing current injection, both of which are consistent with electron recombination in the *p*-type shell layer through donor-acceptor-pair recombination. These core-shell NW devices demonstrate N-polar selective area growth as an effective technique for producing on-chip nanoscale light sources.

**Keywords:** gallium nitride, N-polar, nanowires, light-emitting diodes, core-shell, selective area growth

## 1. INTRODUCTION

Nanowire-based light-emitting diodes (LEDs) offer many exciting possibilities for a host of applications that include silicon-integrated photonics,<sup>1</sup> multi-color pixelated displays,<sup>2, 3</sup> solid-state lighting,<sup>4</sup> and nanoscale light-emitting probes.<sup>5</sup> Nanowire (NW) LEDs with either axial or radial geometries have been reported variously throughout the literature. In most cases, radial core-shell geometries are obtained by metal-organic vapor phase epitaxy (MOVPE) by use of selective area growth techniques,<sup>6</sup> predominantly on patterned Ga-polar GaN templates and to a lesser extent on N-polar substrates.<sup>7, 8</sup> Core-shell structures have the advantage of allowing the active junction area to exceed the device die area. In contrast, NW LEDs produced by molecular beam epitaxy (MBE) have focused primarily on axial structures,<sup>9</sup> both for nanowires grown via self-assembly techniques or by selective area growth (SAG). For self-assembled NWs, which are frequently observed to adopt N-polarity,<sup>9, 10</sup> a lack of direct control over nanowire nucleation typically results in dense NW arrays and precludes conformal shell growth, thus favoring axial structures. Most MBE-based NW LEDs grown via SAG (also primarily on Ga-polar GaN surfaces) have utilized closely spaced nanowire arrays to facilitate surface-diffusion-assisted SAG at lower temperatures. This avoids high-temperature Ga-polar growth limitations associated with SAG,<sup>11</sup> but still produces NW arrays subject to self-shadowing effects similar to self-assembled NWs. Consequently, most NW LED devices to date can be classified into three structural types: Ga-polar core-shell structures (by MOVPE), Ga-polar axial structures (by MBE), and N-polar axial structures (by MBE).

To address the lack of MBE-based growth techniques capable of producing fully conformal and high-aspect ratio core-shell structures, we have developed a highly flexible N-polar selective area nanowire growth process that avoids the self-shadowing effects inherent in MBE.<sup>11</sup> A key feature in this approach is the ability to completely inhibit mask growth while maintaining high nanowire growth rates, allowing fully selective nanowire growth in both dense arrays or in isolated nanowires. As self-shadowing of growth fluxes can be eliminated in isolated nanowires, synthesis of junctions

\*Contribution of an agency of the U.S. government; not subject to copyright.

\*\*matthew.brubaker@nist.gov; phone 1 303 497-4167

or heterostructures with radial geometries is possible. Isolated nanowires also allow for low-temperature growth of the  $p$ -type shell, where Mg incorporation is favored, without coalescence of nanowires. This combination of attributes makes N-polar selective epitaxy by MBE particularly suitable in obtaining core-shell NW LEDs.

In this paper, GaN  $p$ - $i$ - $n$  nanowire LEDs were synthesized via N-polar SAG with an  $n$ -type core and a conformal  $p$ -type shell layer. Electrically contacted LED devices were then fabricated by contacting the  $n$ -type core via the GaN nucleation layer and the  $p$ -type shell via a Ni/Au metallization layer. The optical and electrical characteristics of the LEDs were then measured for single nanowire devices and for arrays comprising multiple nanowire LEDs biased in parallel. It was observed that these devices exhibited the overall behavior expected for functional LEDs – specifically diode-like I-V characteristics and electroluminescence (EL) under forward bias.

## 2. EXPERIMENT

Plasma-assisted MBE was used for growing both the initial N-polar nucleation layers and the subsequent core-shell  $p$ - $i$ - $n$  GaN NWs, which are schematically illustrated in Figure 1. The N-polar AlN/GaN nucleation layers were grown on low-resistivity (0.008-0.025 ohm\*cm)  $n$ -type Si (111) wafers and comprised an  $\approx 20$  nm thick AlN layer, followed by a  $\approx 300$  nm thick GaN layer grown at substrate temperatures of 860 and 700 °C, respectively. N-polarity was induced in the AlN layer by use of Al-rich growth conditions and the top GaN surface was verified N-polar by the appearance of a characteristic 3x3 pattern in the reflection high energy electron diffraction patterns during cooldown.<sup>11</sup> A five period AlGaIn/GaN superlattice (not shown in Figure 1) was used for improving the nucleation layer quality through dislocation filtering. The AlN/GaN nucleation layers were also utilized to provide electrical contact to the  $n$ -type NW cores and were therefore Si doped.

A stoichiometric silicon nitride mask layer was deposited on top of the GaN nucleation layer by low pressure chemical vapor deposition and patterned via electron beam lithography. The silicon nitride layer serves as the growth mask during SAG and provides electrical insulation between the  $n$ -type nucleation layers and the eventual top  $p$ -contact metallization layer. The silicon nitride layer was patterned with hole arrays that have a hexagonal layout, diameters of  $\approx 140$  nm, 5  $\mu$ m spacing between holes, and arrays of various sizes (as shown in Figure 1b). After etching the pattern into the silicon nitride layer with reactive ion etching (RIE), the wafer was thoroughly cleaned and reintroduced to the MBE system.

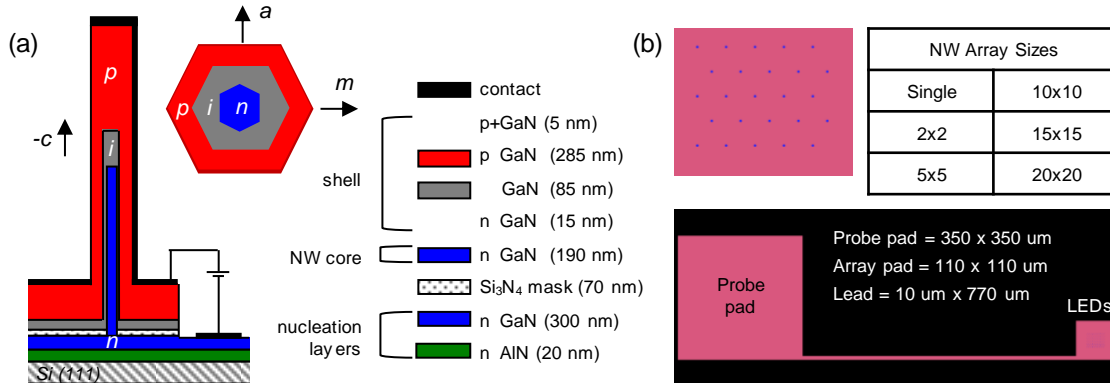


Figure 1. Schematic diagrams showing (a) the cross-sectional structure of core-shell  $p$ - $i$ - $n$  NWs and underlying N-polar nucleation layer and (b) the top-down layout of the NW LED devices. The dimensions in (a) indicate thickness for the planar layers, NW diameter for the core, and radial thickness for the shell. The thin  $p$ + GaIn and  $n$ -GaIn shell layers are omitted from the diagram for clarity. The NW array shown in (b) is the 5x5 array.

The  $n$ -type NW cores were grown at  $\approx 870$  °C, at a nominal planar growth rate of  $\approx 400$  nm/hr, and to dimensions of  $\approx 190$  nm diameter and  $\approx 4$   $\mu$ m length, as estimated from separate growths performed under similar conditions. We note that there are no line-of-sight shadowing effects for NWs of this length and spacing, as the angle of incidence for our effusion sources is 45°. The  $n$ -type NW cores were grown with an initial low-doped  $n$ - section of approximately 160 nm length to reduce current shunting at the NW base. After completion of the NW cores, growth was interrupted for a transition to shell growth conditions at a substrate temperature of  $\approx 700$  °C and a nominal planar growth rate of 80 nm/hr. The radial growth rate under these conditions is  $\approx 35$  % of the nominal planar rate and was used to estimate the following shell layer thicknesses. A 15 nm thick  $n$ -type GaN shell layer was grown to clean up the NW surfaces after

the growth interruption, which was followed by an 85 nm thick undoped *i*-layer and a 285 nm thick Mg-doped *p*-layer. The structure was capped with a final 5 nm thick heavily doped *p*+ layer to assist in fabrication of low-resistance *p*-type contacts.

Contact openings were then patterned and etched to the underlying *n*-type GaN nucleation layer with a chlorine-based RIE process. Lift-off processes were used to deposit 20 nm Ti/300 nm Au *n*-type contacts onto the GaN nucleation layer and in a subsequent step 20 nm Ni/20 nm Pd/400 nm Au *p*-type contacts on top of the GaN NW arrays. The Au deposition for the *p*-contact layer was performed in two steps: the first 200 nm of Au was deposited at 45° incidence and with no substrate rotation to metallize one side of the NWs and the second step was performed at normal incidence and with substrate rotation to ensure electrical conductivity for the *p*-contact pad. A 500 °C contact anneal in Ar was applied after the *n*-contact, but no anneal was used for the *p*-contacts.

The GaN NWs were characterized by scanning electron microscopy (SEM) at various stages in the growth and LED fabrication processes. Electrical testing was performed in a probe station equipped with tungsten probe tips and commercially available electrical test hardware. Spectral measurements were obtained by collecting normal-incidence EL with a UV-transmissive objective that was fiber coupled to a CCD-based spectrometer.

### 3. RESULTS AND DISCUSSION

#### 3.1 Structural Characterization

The structural characteristics of the *n*-type NW cores were investigated by imaging a companion sample grown under similar conditions to the *p-i-n* core-shell NW LEDs. As shown in Figure 2a, selective area core growth produced uniform and hexagonally faceted nanowires that were bounded by *m*-plane sidewalls and flat N-face tips. The substrate temperature was sufficiently high during this step to desorb all impinging species so that no growth occurred on the mask, even in arrays with large pitch spacings (not shown).

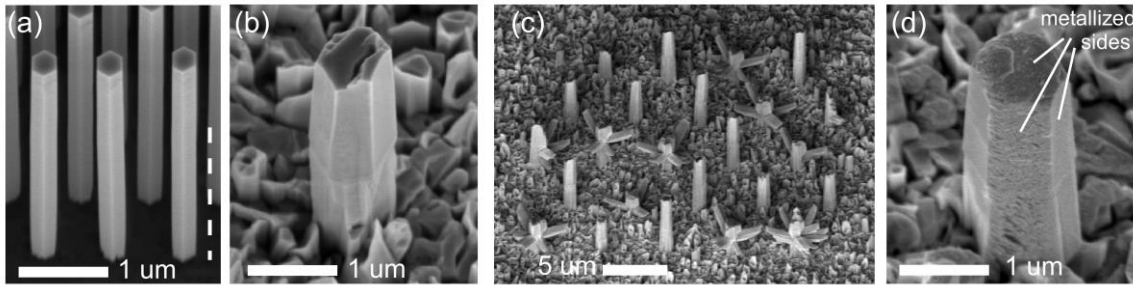


Figure 2. SEM images at 20° tilt from substrate normal showing structure of (a) a 270 nm diameter *n*-type NW core, (b) an as-grown core-shell *p-i-n* NW, (c) an as-grown 5x5 NW array (40° tilt), and (d) a metallized core-shell *p-i-n* NW. The NW cores shown in (a) are from a different sample (and longer growth duration) than the core-shell NWs shown in (b-d). The dotted line in (a) indicates the approximate length of the NW cores in (b-d).

After low-temperature shell growth (Figure 2b), the NWs became significantly thicker and an abrupt change in the sidewall faceting was observed along the NW length. *A*-plane facets emerged at the NW tip and appear rotated by 30° to *m*-plane facets shown in Figure 1a. This transition to *a*-plane faceting is most prominent for the upper section of the NW, where both axial and radial growth would have occurred during the shell layer. The lower section exhibited a more circular cross-section, suggesting an incomplete transition from *m*- to *a*-planes that is likely related to the radial-only growth mode at the NW base. As such, the transition between the circular structure and the *a*-plane facets along the NW length would demarcate the extent of the core in the NW. It should be noted that the *n*-type cores in the NWs shown in Figure 1b-d are approximately 70% shorter than the NW cores shown in Figure 1a (which are from a separate growth run). While the faceting is irregular at the shell surfaces, the interfaces that define the *p-i-n* junction would conform to the more distinct *m*-plane surfaces observed in the NW cores shown in Figure 2a. In some cases, flower-like nanotripod structures were observed after shell growth near the vertical core-to-shell interface, as shown in Figure 2c. These types of structures have been studied by others and were found to initiate on zincblende inclusions that result from reduced Ga mobility at low growth temperatures.<sup>12</sup>

The low temperature used for NW shell growth also caused a loss of selectivity and resulted in growth on the silicon nitride mask surface, as shown in Figures 2b and c. The mask surface growth partially encompassed the bottom section of the nanowire and was estimated to be  $\approx 1 \mu\text{m}$  thick. This rough surface also presented a tradeoff for  $p$ -contact fabrication, where a thick metallization layer would ensure electrical continuity but at the expense of optical transparency for light extraction. Using the two-stage metallization described in the experimental section, the rough layer on the mask, the NW tip surface, and one side of the nanowire were metallized for electrical contact, as shown in Figure 2d. The other NW sidewall was unmetallized for light extraction and EL spectral measurements.

### 3.2 Electrical Characterization

The I-V characteristics of core-shell  $p$ - $i$ - $n$  NW LEDs were measured for devices with varying NW array sizes and rectifying behavior was observed in all cases. As shown in Figure 3a, the devices became forward biased when a positive voltage of 3.4 V was applied to the  $p$ -contact, as expected for a GaN-based LED. In comparing the forward bias curves (which are normalized per NW in Figure 3a), the series resistance was found to increase with the number of NWs in the array. The source of this effect is not presently understood, but could be related to current spreading effects in the  $n$ -type GaN or the  $p$ -contact metallization layers that supply current to the NWs. As shown in Figure 3b, the reverse bias currents are quite low and roughly the same for all devices irrespective of the number of NWs in the array. In fact, the reverse bias currents in these devices appear to be dominated by leakage through the silicon nitride layer, as illustrated by I-V measurements of a blank device with no NWs (indicated by 0 NWs in Figure 3b). A smaller proportion of the leakage current contributed to the per NW I-V characteristics in large-array LED devices, thereby allowing the ideality factor to be determined in the sub-turn-on regime as  $n \approx 2.8$  (Figure 3c). While the textbook values of ideality factor range from  $n=1$  to  $n=2$ , depending on whether carriers recombine in the neutral or depletion regions of the junction, the ideality factors in GaN-based LEDs can frequently be larger due to non-ohmic contacts.<sup>13</sup> We consider the ideality factor measured in these devices to indicate favorable  $p$ -type doping levels and low contact resistances, despite the lack of a  $p$ -contact anneal.

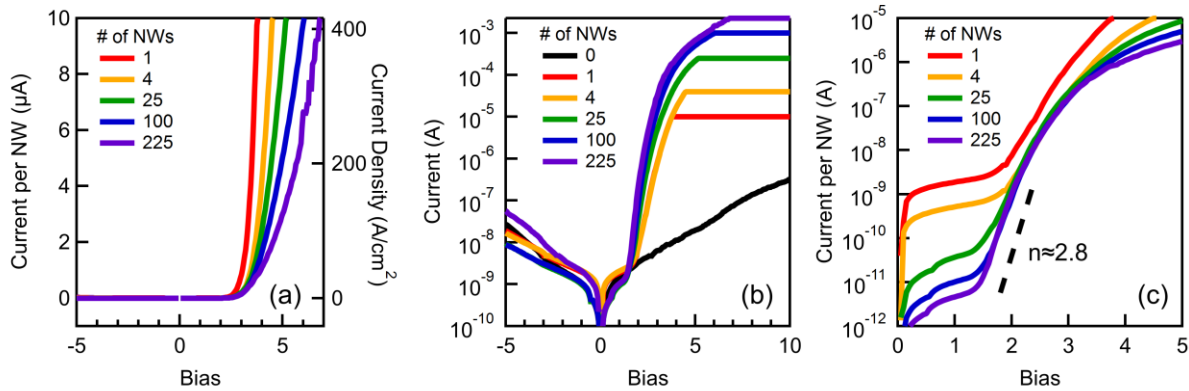


Figure 3. I-V characteristics of NW LED array devices showing (a) linear current per NW, (b) total log current for the array, and (c) log current per NW. The bias indicated in the plots was applied to the  $p$ -contact and the  $n$ -contact was held at ground potential. The current density in (a) represents the current scaled by the  $n$ -type NW core surface area and the number of NWs per device is indicated in the figure legends. The maximum current was limited to  $10 \mu\text{A/NW}$ , producing the horizontal lines at high bias conditions shown in (b).

### 3.3 Optical Characterization

Electroluminescence spectra were obtained for core-shell GaN NW  $p$ - $i$ - $n$  LEDs with varying array sizes and Figure 4a shows the spectra for a typical device at increasing current injection levels. The spectra under forward bias display a peak wavelength near 380 nm and a full-width at half-maximum (FWHM) of approximately 30 nm. No yellow luminescence was observed in the spectra (not shown). The overall intensity (shown in Figure 4b) increased linearly with forward bias injection current, while the peak wavelength shifted towards shorter wavelengths by  $\approx 5$  nm. Interestingly, electroluminescence is observed to originate from the individual NWs in the array (as shown in Figure 4c), despite the thick metallization layer on the NW tip. Some diffuse luminescence is observed in the larger arrays and might correspond to non-uniform emission from the non-metallized sidewall surfaces or from the fraction of NWs with the nanotripod structures shown in Figure 2c.

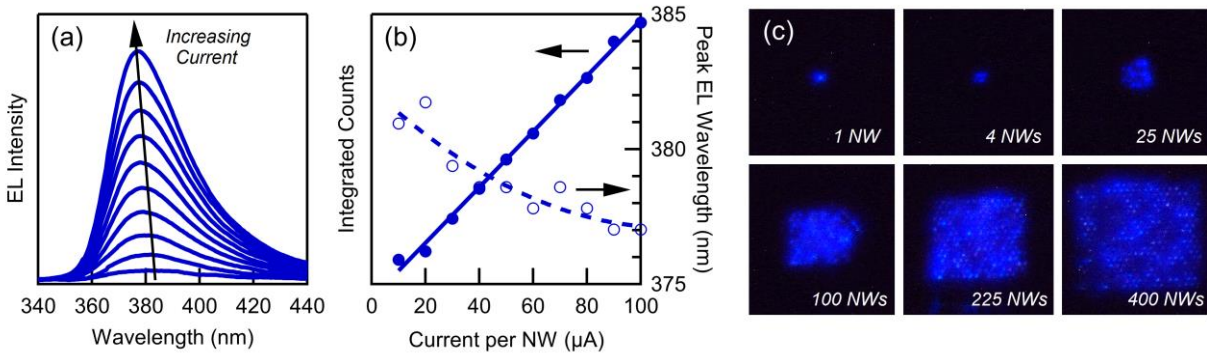


Figure 4. Optical characteristics of core-shell  $p$ - $i$ - $n$  GaN NW LEDs showing (a) EL spectra for a  $5 \times 5$  (25 NW) LED array device under increasing forward bias current injection, (b) integrated spectral counts and peak wavelength versus current injection level and (c) EL images for various LED array sizes. The current injection levels shown in (b) correspond to those shown in the EL spectra shown in (a). The lines shown in (b) are curve fits to guide the eye.

While the emission wavelength of a GaN-based LED might be expected to correspond to the GaN band-edge at 365 nm, carrier recombination in heavily-Mg-doped GaN typically occurs via Mg-related localized states producing donor-acceptor-pair (DAP) recombination at 380 nm.<sup>14</sup> Electron injection into the  $p$ -type shell would produce DAP emission, whereas holes injected into the  $n$ -type core would produce GaN band-edge emission. However, the shorter-wavelength emission from the GaN core would be reabsorbed by the thick  $p$ -type shell and would not contribute to the spectra. Moreover, the spectral blueshift with increasing current injection in these LEDs is consistent with excitation-intensity-dependent photoluminescence studies reported elsewhere for Mg:GaN layers.<sup>14</sup> We note that quantum confined Stark effects can be ruled out as there are no quantum wells or heterostructures in these GaN-based homojunction LEDs. Similarly, Varshni shifts related to device self-heating cannot be considered as a primary effect here, as this would result in a redshift of the EL spectra with increasing current instead of the observed blueshift.

#### 4. SUMMARY AND CONCLUSIONS

We have demonstrated core-shell GaN NW  $p$ - $i$ - $n$  LEDs grown by MBE, making use of an N-polar SAG technique. This highly flexible process facilitates the growth of isolated high-aspect ratio NWs, which are not subject to line-of-sight shadowing effects during low-temperature  $p$ -type shell growth. As such, the resulting  $p$ -shells are fully conformal and can be metallized directly without shorting to the underlying layers, so long as an electrically insulating growth mask is used. The NW LEDs exhibit clear diode-like electrical properties including turn-on voltage near 3.4 V, low reverse bias leakage current, and ideality factor of  $\approx 2.8$ . Similarly, the EL spectra exhibit clear behavior that includes spectral emission at 380 nm, which corresponds to DAP recombination from electrons injected into the  $p$ -shell and a linear correspondence between the injected current and the total luminosity. A small spectral blueshift was observed with increasing current injection similar to excitation-dependent photoluminescence studies reported by others.<sup>14</sup> In conclusion, these  $p$ - $i$ - $n$  NW LEDs are expected to pave the way for higher-efficiency designs based on quantum wells and for applications requiring on-chip nanoscale light sources.

#### REFERENCES

- [1] P. D. Yang, R. X. Yan, and M. Fardy, "Semiconductor Nanowire: What's Next?," *Nano Letters*, 10(5), 1529-1536 (2010).
- [2] K. Kishino, K. Nagashima, and K. Yamano, "Monolithic Integration of InGaN-Based Nanocolumn Light-Emitting Diodes with Different Emission Colors," *Applied Physics Express*, 6(1), (2013).
- [3] Y. H. Ra, R. J. Wang, S. Y. Woo, M. Djavid, S. M. Sadaf, J. Lee, G. A. Botton, and Z. T. Mi, "Full-Color Single Nanowire Pixels for Projection Displays," *Nano Letters*, 16(7), 4608-4615 (2016).
- [4] S. F. Li, and A. Waag, "GaN based nanorods for solid state lighting," *Journal of Applied Physics*, 111(7), (2012).

- [5] K. A. Bertness, N. A. Sanford, P. Kabos, and T. M. Wallis, "Tip-mounted nanowire light source instrumentation," US Patent US8484756B2 (2013).
- [6] S. F. Li, [Radial GaN Nanowire-based LEDs in Wide band gap semiconductor nanowires] ISTE; John Wiley & Sons, Inc., London, UK, Hoboken, NJ, 135-159 (2014).
- [7] A. Waag, X. Wang, S. Fundling, J. Ledig, M. Erenburg, R. Neumann, M. Al Suleiman, S. Merzsch, J. D. Wei, S. F. Li, H. H. Wehmann, W. Bergbauer, M. Strassburg, A. Trampert, U. Jahn, and H. Riechert, "The nanorod approach: GaN NanoLEDs for solid state lighting," *Physica Status Solidi C: Current Topics in Solid State Physics*, Vol 8, No 7-8, 8(7-8), (2011).
- [8] P. Tchoulfian, F. Donatini, F. Levy, A. Dussaigne, P. Ferret, and J. Pernot, "Direct Imaging of p-n Junction in Core-Shell GaN Wires," *Nano Letters*, 14(6), 3491-3498 (2014).
- [9] S. R. Zhao, H. P. T. Nguyen, M. G. Kibria, and Z. T. Mi, "III-Nitride nanowire optoelectronics," *Progress in Quantum Electronics*, 44, 14-68 (2015).
- [10] M. D. Brubaker, A. Roshko, P. T. Blanchard, T. E. Harvey, N. A. Sanford, and K. A. Bertness, "Spontaneous growth of GaN nanowire nuclei on N- and Al-polar AlN: A piezoresponse force microscopy study of crystallographic polarity," *Materials Science in Semiconductor Processing*, 55, 67-71 (2016).
- [11] M. D. Brubaker, S. M. Duff, T. E. Harvey, P. T. Blanchard, A. Roshko, A. W. Sanders, N. A. Sanford, and K. A. Bertness, "Polarity-Controlled GaN/AlN Nucleation Layers for Selective-Area Growth of GaN Nanowire Arrays on Si(111) Substrates by Molecular Beam Epitaxy," *Crystal Growth & Design*, 16(2), 596-604 (2016).
- [12] P. Wang, X. Q. Wang, T. Wang, C. S. Tan, B. W. Sheng, X. X. Sun, M. Li, X. Rong, X. T. Zheng, Z. Y. Chen, X. L. Yang, F. J. Xu, Z. X. Qin, J. Zhang, X. X. Zhang, and B. Shen, "Lattice-Symmetry-Driven Epitaxy of Hierarchical GaN Nanotripods," *Advanced Functional Materials*, 27(9), (2017).
- [13] J. M. Shah, Y. L. Li, T. Gessmann, and E. F. Schubert, "Experimental analysis and theoretical model for anomalously high ideality factors ( $n \gg 2.0$ ) in AlGaIn/GaN p-n junction diodes," *Journal of Applied Physics*, 94(4), 2627-2630 (2003).
- [14] M. A. Reshchikov, and H. Morkoc, "Luminescence properties of defects in GaN," *Journal of Applied Physics*, 97(6), (2005).